Fluctuating Pressure Environment of a Drag Reduction Spike

Rolf A. Guenther* and J. Peter Reding†
Lockheed Missiles & Space Company, Inc., Sunnyvale, Calif.

Wind-tunnel measurements have been made of the fluctuating pressure environment in a region of spike-induced flow separation. Extremely large pressure fluctuations (30% of freestream dynamic pressure) were measured on the sides of the spike base at transonic speeds which are related to the nonaxisymmetric, vortical nature of the separated flow at $\alpha > 0$. Even higher (42% of freestream dynamic pressure) pressure fluctuations were observed on the windward side of the nose cap at supersonic speeds and $\alpha \geq 7$ deg. This is the result of an intermittent shock-shock interaction. The method of Coe et al. of normalizing the spectral data with the local separated flow height was moderately successful in collapsing the data into a manageable number of characteristic spectra. However, the spectra for the spike-induced separation at supersonic speeds agreed better with the results of Speaker and Ailman for two-dimensional step-induced separation than they did with the three-dimensional ramp-induced separation of Coe et al. Spectral peaks were observed which corresponded to Roberts' critical subsonic wake flapping frequency.

Nomenclature

a	= speed of sound
C_P	= static pressure coefficient ($C_P = \lvert P - P_\infty \rvert / q_\infty$)
ΔC_P	= incremental pressure coefficient ($C_P = \Delta P / q_\infty$)
f	= frequency, Hz
L_s	= spike length
M	= freestream Mach number ($M = V_\infty / a$)
P	= pressure
ΔP	= incremental pressure
PSD	= power spectral density
rms	= root-mean-square
q_∞	= freestream dynamic pressure $q_\infty = (\rho V_\infty{}^2)/2$
V_∞	= freestream velocity
x	= axial distance
α	= angle of attack
δ	= disturbed flow height
ρ	= freestream density

Introduction

THE Trident I missile features an extendible nose spike that reduces the drag of the blunt nose by creating a low-dynamic-pressure flow separation (Figs. 1 and 2). The lower dynamic pressure within the region of spike-induced separation results in reduced static pressure (Fig. 3), accounting for the drag reduction

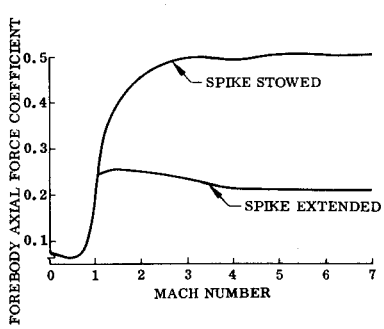

Fig. 1 Effect of spike on $\alpha = 0$ axial force coefficient.

It is well known that elevated fluctuating pressures occur in regions of flow separation. The telescoping design of the aerospike was considered to render its structural dynamic response particularly vulnerable to an aggravated fluctuating pressure environment. Thus, wind-tunnel tests were conducted at the Arnold Engineering Development Center 16-ft transonic wind tunnel and the NASA Lewis Research Center 10- × 10-ft supersonic wind tunnel on a subscale aerospike-nose fairing model (Fig. 4).[1] The model was equipped with 66 fluctuating pressure transducers, 83 static pressure orifices, boundary-layer rakes, and an internal roll capability. The nose cap and spike were constructed of heavy-gage stainless steel to eliminate model vibrations and the attendant accelerations that could contaminate the fluctuating pressure data. An analysis of the significant wind-tunnel results is presented herein.‡

Overall Fluctuating Pressure Distribution

On the nose cap, the overall fluctuating pressure coefficient $\Delta C_{P(\text{rms})}$ distribution generally correlates well with the static

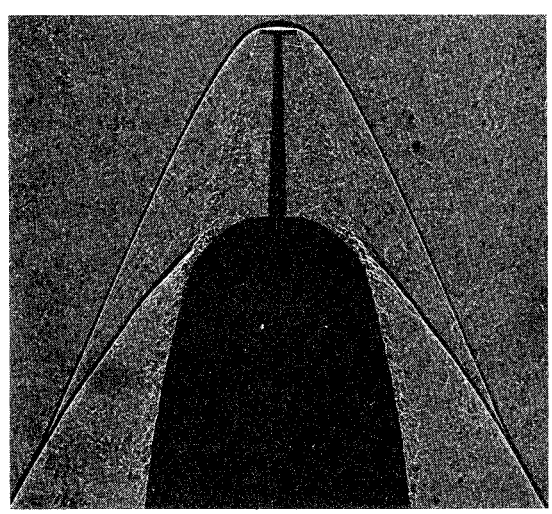

Fig. 2 Trident 1, $M = 3.0$.

Presented as Paper 77-90 at the AIAA 15th Aerospace Sciences Meeting, Los Angeles, Calif., Jan. 24-26, 1977; submitted Feb. 8, 1977; revision received Aug. 8, 1977.

Index categories: Viscous Nonboundary-Layer Flows; Jets, Wakes, and Viscid-Inviscid Flow Interaction; Nonsteady Aerodynamics.

*Aerodynamics Engineer Sr.

†Research Specialist. Member AIAA.

‡These tests were conducted at the maximum Reynolds number capabilities of the facilities based on the model blockage. For the transonic test, this corresponds to a Reynolds number range based on model spike length of 6.92 × 10^6 to 10.4 × 10^6 and to supersonic speeds from 4.15 to 6.06 × 10^6.

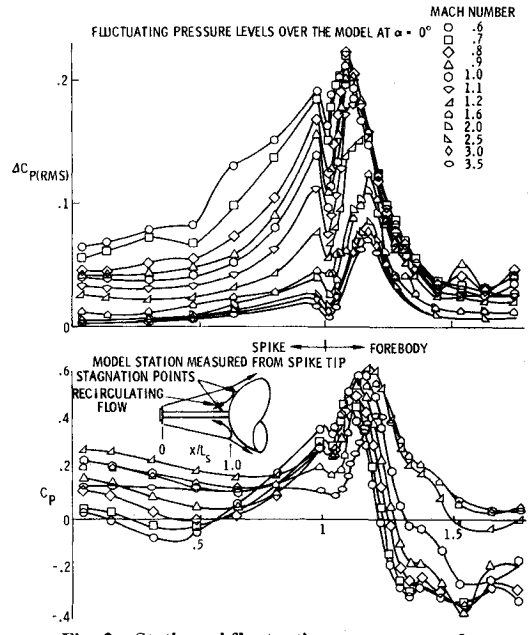

Fig. 3 Static and fluctuating pressure, $\alpha = 0$.

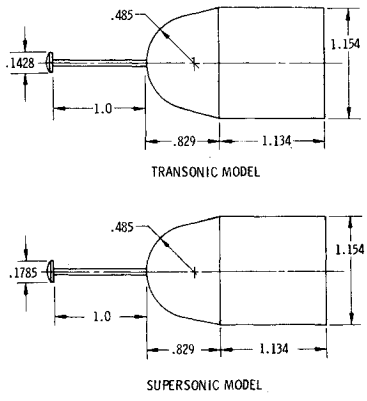

Fig. 4 Model configuration.

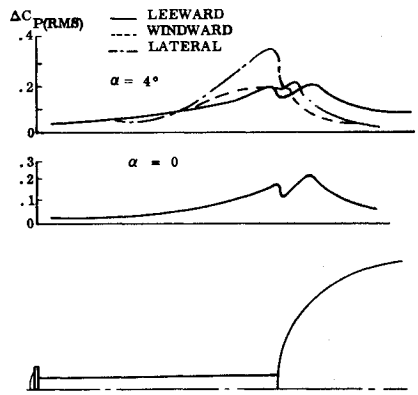

Fig. 5 Fluctuating pressure distributions at $M = 0.8$.

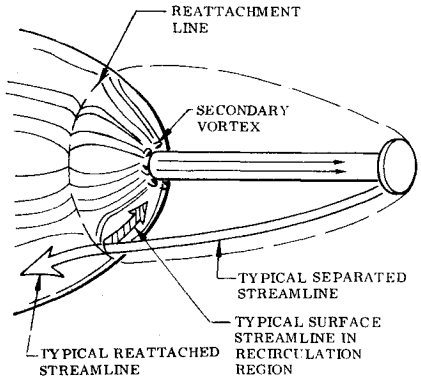

Fig. 6 Spike-induced flowfield for $\alpha = 0$.

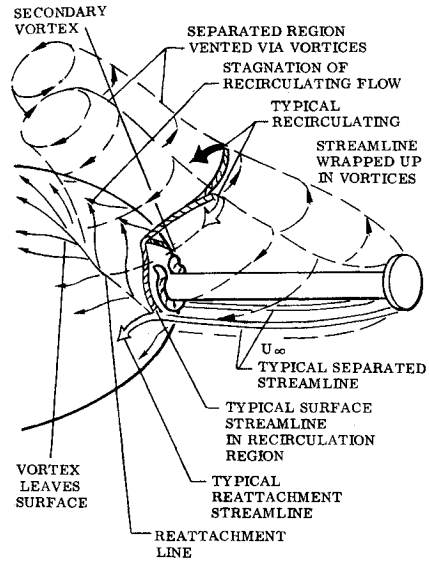

Fig. 7 Spike-induced flowfield for $\alpha > 0$.

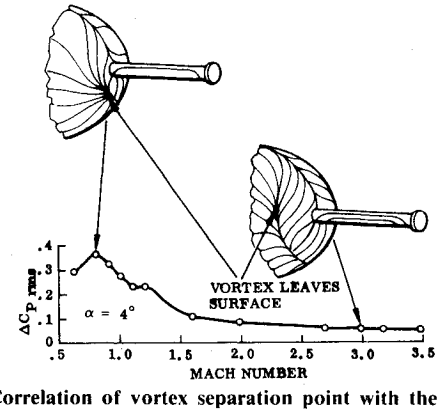

Fig. 8 Correlation of vortex separation point with the fluctuating pressures on the side of the spike base at $\alpha = 4$ deg.

pressure coefficient C_P distribution, with the peak pressure fluctuations occurring at reattachment (Fig. 3). Likewise, the regions of high-pressure fluctuations at the rear (or base) of the spike correlate with peaks in the static pressure distribution. However, this correlation does not hold over the forward portions of the spike. The fluctuating pressures decrease monotonically with increasing Mach number on the forward spike, whereas the static pressures increase with increasing Mach number up to $M = 1.2$ and decrease to a relative constant at $M \geq 2.5$ (Fig. 3). This is because the separated region is a complicated merging of the wake from the spike disk and the step-induced separation forward of the nose cap.

The aerospike was designed to minimize nose drag at supersonic speeds where the dynamic pressure is high and the drag penalty significant. The disk tip was found to give a larger drag reduction than could be obtained with a pure (untipped) spike.[2] However, the tip produces a complicated merged flowfield where the wake from the disk merges with the step (or conventional spike) induced separation and forms a separated region that is larger than either region would be alone. At subsonic speeds, the step-induced separation is small and may not link up with the disk wake. This occurs at

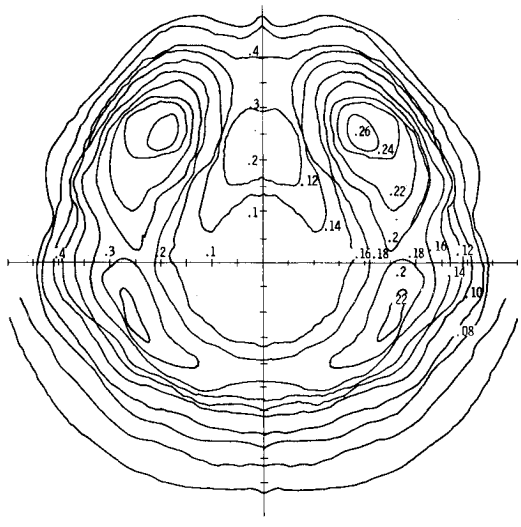

a) $\Delta C_{P(\mathrm{rms})} = \mathrm{const}$

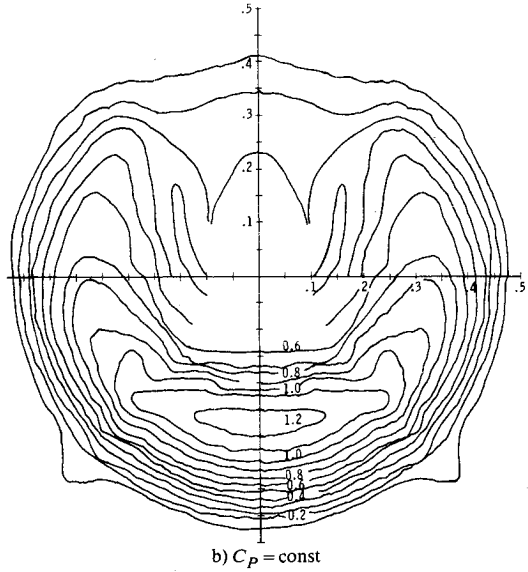

b) $C_P = \mathrm{const}$

Fig. 9 $M = 1.2$ isobars, $\alpha = 4$ deg.

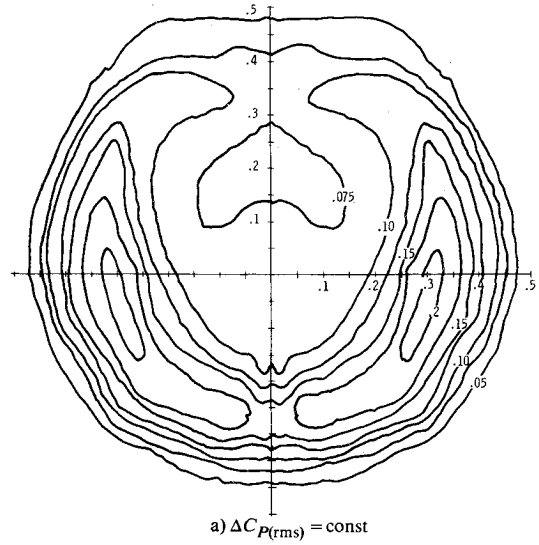

a) $\Delta C_{P(\mathrm{rms})} = \mathrm{const}$

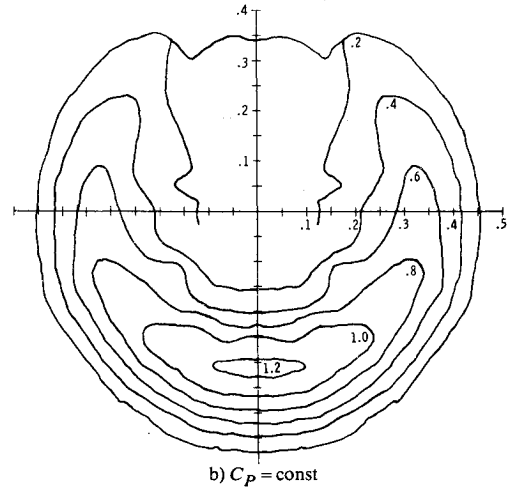

b) $C_P = \mathrm{const}$

Fig. 10 $M = 1.6$ isobars, $\alpha = 4$ deg.

$M = 0.6$, where the disk wake begins to reattach on the spike at about $x/L_s = 0.4$, as indicated by the upturn in the C_P curve. The fluctuating pressures are high in the unstabilized wake and rise rapidly in the reattachment region over the aft spike. The spike wake may alternately merge and separate from the step-induced separation, which may explain the equally high fluctuating pressure on spike base and nose cap. A secondary vortex occurs at the spike-nose cap juncture which is responsible for the pervasive valley in both C_P and $\Delta C_{P(\mathrm{rms})}$ plots.§

At $M = 0.8$, reattachment occurs on the nose cap very near the spike base, as reflected by the peak static and fluctuating pressures on the nose cap along with the very high values at the spike base. As the Mach number increases, the dominance of the step-induced separation grows. Reattachment moves aft on the nose fairing, and the separation angle becomes steeper (as indicated on Fig. 3). The fluctuating pressures along the spike decrease as the source (the shear layer) moves away from the spike shaft.

Perhaps the single most surprising result of these tests is indicated in Fig. 5. At transonic speed and moderate angle of attack, the peak pressure fluctuations occurred on the lateral meridian of the spike near the spike base; oil flow visualization results[3] show that the spike-induced separation at $\alpha = 0$ is a closed, axisymmetric, recirculating flow with a secondary vortex at the spike-nose cap juncture (Fig. 6). However, for $\alpha > 0$, the separated region is neither axisymmetric nor closed (Fig. 7). The separation region resembles a horseshoe vortex, with the two counter-rotating legs of the horseshoe venting the separated region and shedding over the shoulder. The points where the vortex leaves the surface are indicated by the sourcelike oil streaks that terminate the feathery reattachment line. The points appear to be the key to the elevated fluctuating pressures on the spike sides. At transonic speeds, where the fluctuating pressures on the spike sides are high, the streak lines eminating from the vortex detachment points impinge on the spike sides; whereas, at supersonic speeds, where the fluctuating pressures on the spike sides are low, the streak lines from the vortex detachment point miss the spike altogether (Fig. 8). It is believed that the flow impinging from the vortex detachment point interacts with the secondary vortex to produce the high-pressure fluctuations on the spike sides.

There are clearly two pairs of fluctuating pressure peaks (Fig. 9a). The windward peaks roughly correspond with the lateral terminus of the reattachment line, as indicated by the rapid decrease in the windward side static pressure peak (Fig. 9b). This is the vortex detachment point. The leeside fluctuating pressure peaks have no corresponding static pressure peak. They do, however, correspond to the point of closest approach of the shed horseshoe vortex legs. Furthermore,

§Oil flow results discussed later also indicate the secondary vortex.

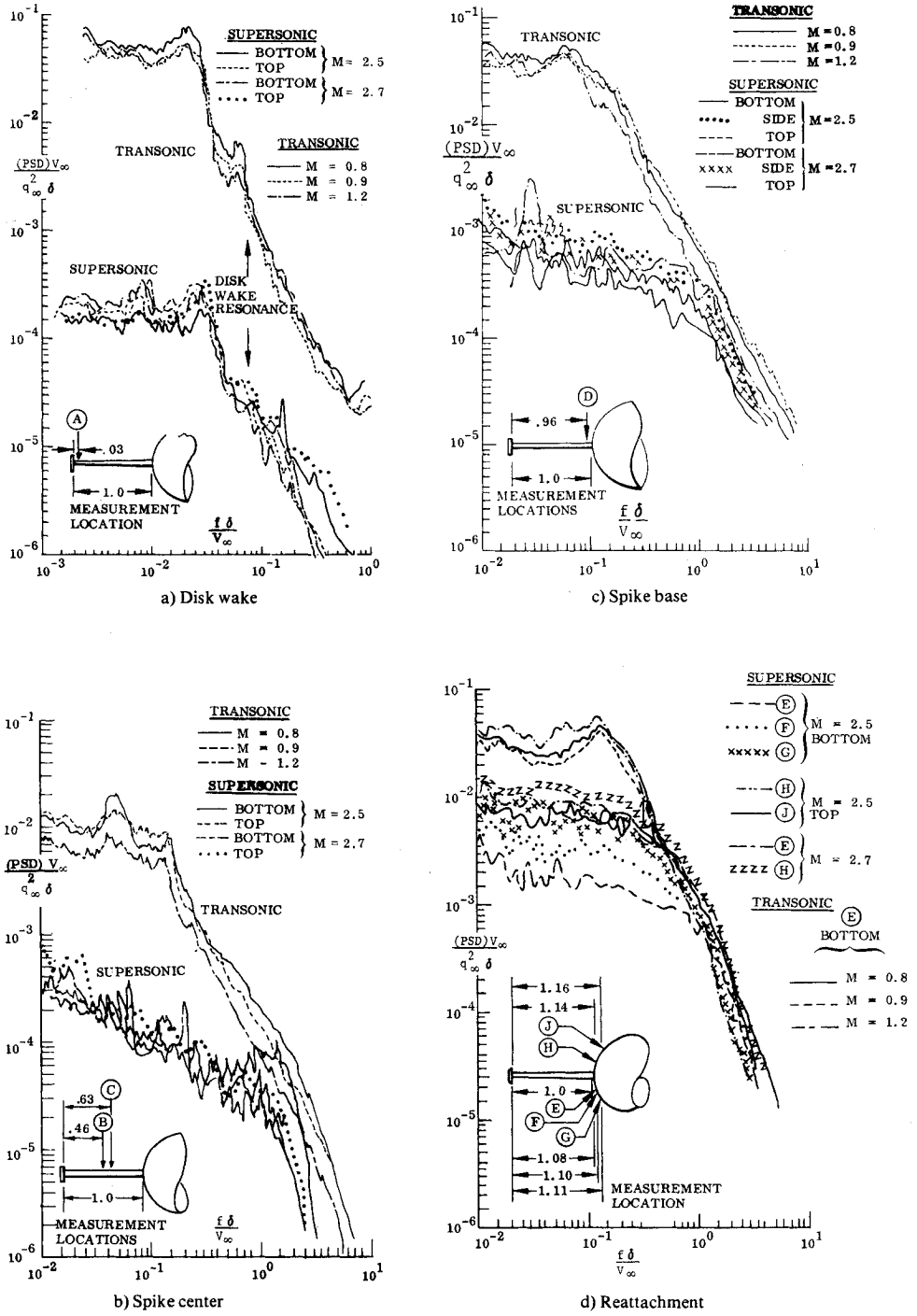

Fig. 11 $\alpha = 0$ **spectra.**

shadowgraph photographs indicate major eruptions¶ of the separated flow in the vicinity of these peaks which could be indicative of vortex burst due to the grazing impingement of the horseshoe vortex legs on the leeside nose cap.

At $M = 1.6$, the leeward fluctuating pressure peaks disappear (Fig. 10a), and only the peaks at vortex detachment remain. These correlate with the lateral terminus of the reattachment shock or the sudden falloff of the windward side static pressure peak (Fig. 10b). Obviously the spike flow is stabilized at supersonic speeds. Vortex burst due to impingement is unlikely, since the vortex separates from the lateral meridian of the nose cap. This is verified by the more regular shadowgraph patterns at supersonic speeds ($M \geq 1.6$).

¶Unfortunately, these photographs are of too poor a quality to survive reproduction herein.

Power Spectra

In order to facilitate scaling the data to full-scale flight conditions, the power spectra were nondimensionalized using the Coe et al. technique of considering the local separated flow height as the proper scaling length.[4,5] This successfully reduced the number of spectral types within the separated region at $\alpha = 0$ to four for transonic and supersonic speeds, respectively (Fig. 11). That the spike-induced separated flow is a complex merging of the wake flow from the tip and the step-induced separation forward of the nose cap is illustrated by the spectra. Disk wake and reattachment spectra represent the two end conditions. The reattachment spectra actually characterize the entire flow over the nose cap within the separated region. The spectra at the spike base are very similar to the reattachment spectra, which is indicative of strong

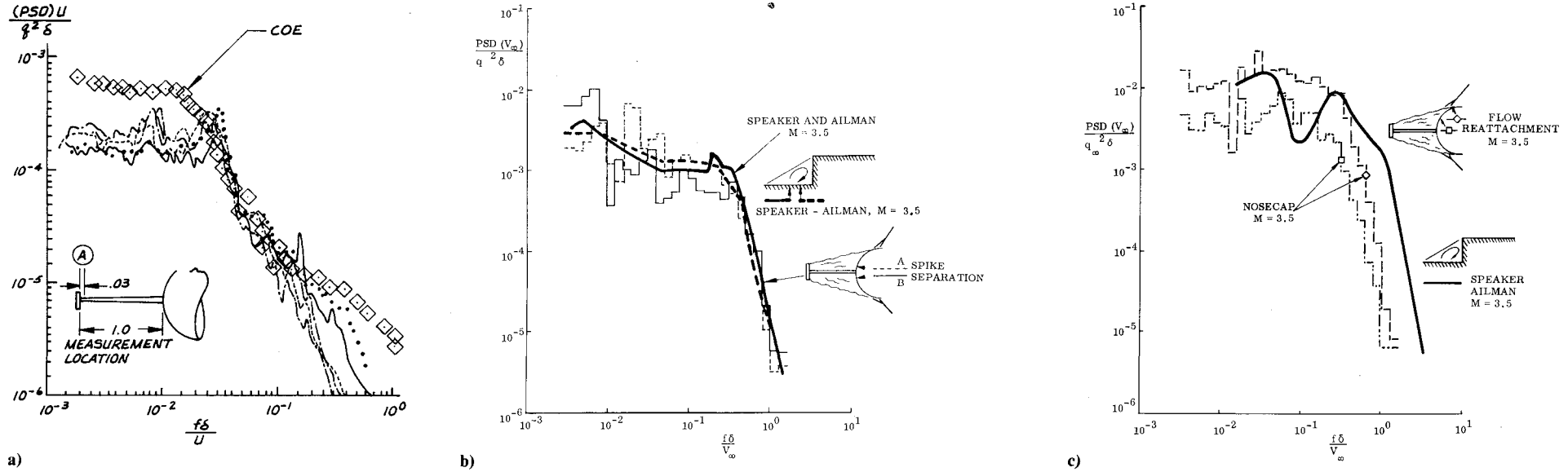

Fig. 12 Comparison of spectra: a) separation point, b) recirculation region, c) reattachment.

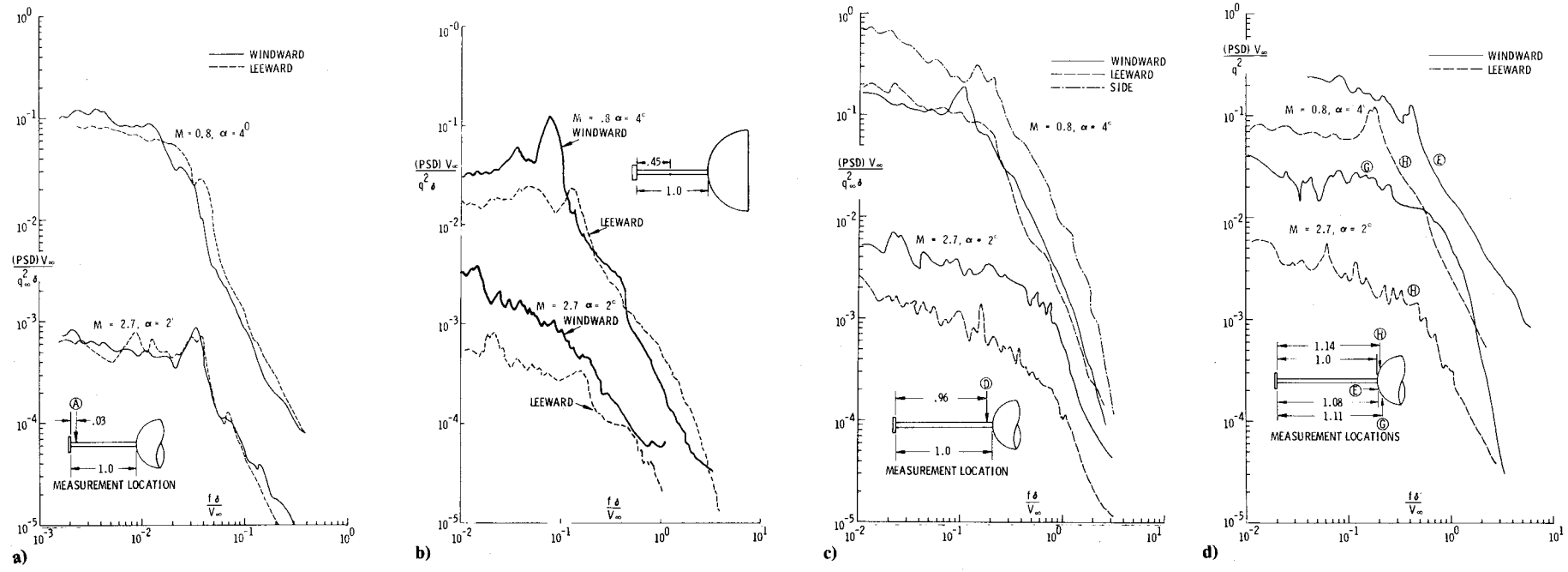

Fig. 13 Typical $\alpha > 0$ spectra: a) disk wake, b) spike center, c) spike base, d) reattachment.

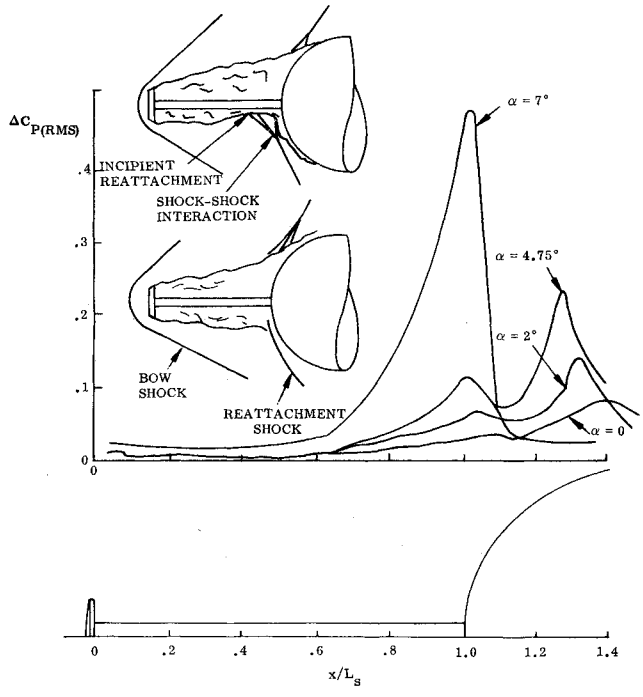

Fig. 14 Effect of on-off shock-shock interaction at $M = 2.7$.

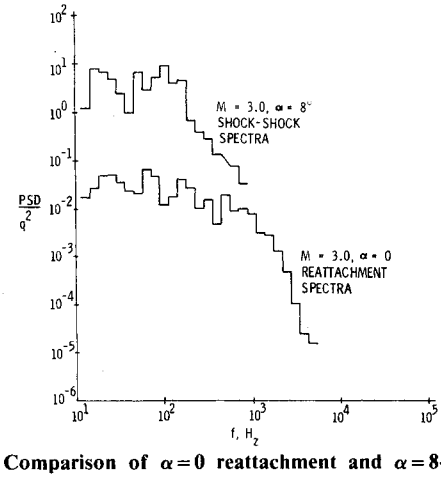

Fig. 15 Comparison of $\alpha = 0$ reattachment and $\alpha = 8$-deg shock-shock spectra.

coupling between the two regions. Likewise, the disk wake seems to dominate the spike center.

At transonic speed, the disk wake shows a peak that correlates well with Roberts' critical subsonic wake flapping frequency (Fig. 11a).[6] Since the peak is small, there is only a slight tendency for flapping. However, this tends to verify the wakelike nature of the flow aft of the disk.

The comparison of intermittent shock data in the flare-induced separated flowfield of Coe ($M = 2$) and the disk wake ($M = 2.5$-2.7) shows good agreement except at low frequencies. For Coe's flowfield, the movement of the separation shock wave produces the low-frequency noise, whereas in the present flow the low-frequency noise is caused by the random passage of shocklets generated by the eddies shed from the disk. The attenuation between the shock interaction and the surface is less for Coe's data, since the turbulent boundary layer is thinner than is the separated region of the present flowfield. Therefore, it is expected that the present data should lie below Coe's at low frequencies, as is shown in Fig. 12a. The spike-induced separation data agree better with the two-dimensional step-induced data of Speaker and Ailman (Fig. 12).[7] They observed a strong lateral flow component parallel to the step. Thus, even though their model was two-dimensional, the flow was strongly three-dimensional. This may explain the better agreement with the present spike results.

At angle of attack, there is a distinct difference between windward and leeward side spectra all along the spike and nose cap except for the region just aft of the disk (Fig. 13). Transonic and supersonic spectra remain distinctly different.

The highest fluctuating pressures measured were observed on the windward side of the nose cap at supersonic speeds (Fig. 14). Shadowgraph photographs indicate that this is the result of an on/off concavity in the separation just forward of the nose cap. The oblique shock that eminates from the concavity intercepts the reattachment shock, thus greatly enhancing the reattachment pressure fluctuations.** The concavity is believed to be indicative of the flow from the disk wake just reattaching on the spike and immediately reseparating due to the increased pressure resulting from the bow-shock wave on the nose. A further increase in angle of attack should result in distinctly separate disk-wake and step-induced separated flow regions. The shock-shock interaction results in a peak in the nondimensionalized PSD at low frequencies and an overall magnification (or constant ratio) in the reattachment spectra throughout the higher frequencies (Fig. 15).

Conclusions

Detailed fluctuating pressure measurements in a region of flow separation induced by a disk-tipped, flow separation spike indicate a merged flowfield that exhibits disk-wake and step-induced separation properties. Extremely large pressure fluctuations occur on the spike sides at transonic speeds which appear to be related to the detachment of the vortices that vent the separated region at angle of attack. The maximum measured pressure fluctuations were the result of a shock-shock interaction due to incipient reattachment of the disk wake on the spike at supersonic speeds. The technique of Coe et al. of nondimensionalizing the spectra with the local separation height was moderately successful in collapsing the data. However, the spike-induced separation spectra resembled the step-induced separation results of Speaker and Ailman.

References

[1] Guenther, R.A., "Analysis of the Fluctuating Pressure Test of the C4A Candidate Nose Fairing," Lockheed Missiles and Space Co., LMSC/D366982, 1975.

[2] Ericsson, L.E. and Reding, J.P., "Dynamics of Separated Flow Over Blunt Bodies," Lockheed Missiles and Space Co., LMSC-2-80-65-1, 1965.

[3] French, N.J. and Jecmen, D.M., "Transonic/Supersonic Wind Tunnel Investigation of Effects of Parametric Variations in Nose Fairing and Aerospike Geometry on Trident I C4 Missile Body Static Stability and Drag (C4A-1, E-78), (C4A-1, E-79)," Lockheed Missiles and Space Co., TM 81-11/77, LMSC/D366908, 1974.

[4] Coe, C.F., "Surface Pressure Fluctuations Associated with Aerodynamic Noise," *Basic Aerodynamic Nose Research*, NASA SP-207, July 1969, pp. 409-424.

[5] Coe, C.F. and Chu, W.J., "Pressure-Fluctuation Inputs and Response of Panels Underlying Attached and Separated Supersonic Turbulent Boundary Layers," NASA TM X-62, 189, Sept. 1972.

[6] Roberts, J.B., "Coherence Measurements in an Axisymmetric Wake," *AIAA Journal*, Vol. 11, Nov. 1973, pp. 1569-1571.

[7] Speaker, W.V. and Ailman, C.M., "Static and Fluctuation Pressures in Regions of Separated Flow," AIAA Paper 66-456, June 1966.

[8] Edney, B.E., "Effects of Shock Impingement on the Heat Transfer Around Blunt Bodies," *AIAA Journal*, Vol. 6, Jan. 1968, pp. 15-21.

**Such interactions are known to increase both static pressure and heating environments as well.[8]